JOURNAL OF MATERIALS SCIENCE **34** (1999) 3875–3882

Slow crack growth analysis of brittle materials with finite thickness subjected to constant stress-rate flexural loading

S. R. CHOI*
Cleveland State University, Cleveland, OH 44115
E-mail: sung.r.choi@lerc.nasa.gov

J. P. GYEKENYESI
NASA Lewis Research Center, Cleveland, OH 44135

A two-dimensional, numerical analysis of slow crack growth (SCG) was performed for brittle materials with finite thickness subjected to constant stress-rate ("dynamic fatigue") loading in flexure. The numerical solution showed that the conventional, simple, one-dimensional analytical solution can be used with a maximum error of about 5% in determining the SCG parameters of a brittle material with the conditions of a normalized thickness (a ratio of specimen thickness to initial crack size) $T > 3.3$ and of a SCG parameter $n \geq 10$. The change in crack shape from semicircular to elliptical configurations was significant particularly at both low stress rate and low T, attributed to predominant difference in stress intensity factor along the crack front. The numerical solution of SCG parameters was supported within the experimental range by the data obtained from constant stress-rate flexural testing for soda-lime glass microslides at ambient temperature.

1. Introduction

Constant stress-rate (also called "dynamic fatigue") testing has been utilized for several decades to quantify the slow crack growth behavior of glass and ceramic materials at both ambient and elevated temperatures [1–7]. The merit of constant stress-rate testing over other methods lies in its simplicity: Strengths are determined in a routine manner at four to five stress rates by applying constant crosshead speeds (displacement-control) or constant loading rates (load-control). The slow crack growth (SCG) parameters required for life prediction/reliability are simply calculated from a relationship between failure strength and stress rate. Because of its advantages, constant stress-rate flexural testing has been developed as an ASTM test standard (C 1368) to determine SCG parameters of advanced ceramics at ambient temperature [8].

The slow crack growth analysis of brittle materials containing surface cracks under constant stress-rate loading condition has been made for the natural flaw system [1] as well as the indentation-induced flaw systems [9–11]. In both cases, the typical assumption in the analyses was that critical crack sizes at failure, after subsequent slow crack growth, are much smaller than specimen size, considering the specimen as an infinite body as compared to crack sizes. In reality, however, the crack sizes cannot be always small relative to the specimen sizes, particularly for finite, thin specimens such as glass microslides ($\leq$1 mm thick) or thin ceramic plates. This is especially true for a material exhibiting a high SCG susceptibility (i.e., with a low SCG parameter of $n < 20$): The critical crack size at high stress rates of the order of 10^1 to 10^2 MPa/s may be small with respect to the specimen thickness; whereas, the critical crack size at low stress rates of the order of 10^{-2} to 10^{-3} MPa/s would be more comparable to the specimen thickness, due to enhanced slow crack growth.

Furthermore, at these low stress rates particularly *in flexure*, the stress intensity factor at the crack surface would be greater than that at the crack depth (due to a stress gradient through the thickness), resulting in a faster crack growth in the surface than in the depth direction. As a result, a change in crack shape into an elliptical crack configuration is inevitable. The solution in this case requires a two-dimensional, numerical slow-crack growth approach in which each individual crack velocity is to be specified at each individual crack front, coupled with the corresponding time-varying stress intensity factor. Such a two-dimensional analysis, however, has not been yet applied to finite, thin glass or ceramic specimens subjected to constant stress-rate condition. Only conventional, one-dimensional, infinite-body analytical solution has been commonly utilized [1–11].

The main objective of this work was to investigate analytically (numerically) how finite specimen thickness

* Corresponding author: NASA Lewis Research Center, Cleveland, OH 44135.

relative to crack size has an effect on the determination of SCG parameters in constant stress-rate loading in flexure. A two-dimensional numerical analysis was performed to determine both SCG parameters and crack shape. Four different specimen thicknesses with respect to initial crack sizes were used in the analysis. Limited constant stress-rate ("dynamic fatigue") testing were conducted in flexure using thin sodalime glass microslides with four different sizes of surface cracks in order to compare the numerical solution with experimental data.

2. Analysis

In many cases, slow crack growth of glass and ceramics under mode I loading above the fatigue limit is described by the following empirical power-law relation [12]:

$$v = \frac{da}{dt} = A\left(\frac{K_I}{K_{IC}}\right)^n \tag{1}$$

where v, a, t are crack velocity, crack size, and time, respectively. A and n are the material/environment-dependent SCG parameters. K_I is the mode I stress intensity factor (SIF), and K_{IC} is the critical stress intensity factor or fracture toughness of the material, subjected to mode I loading. Under constant stress-rate ("dynamic fatigue") loading using either constant displacement rate or constant loading rate, the corresponding failure strength (σ_f) based on an infinite-body assumption can be derived as a function of stress rate ($\dot{\sigma}$) as follows [1]:

$$\sigma_f = \left[B(n+1)\sigma_m^{n-2}\right]^{1/(n+1)}\dot{\sigma}^{1/(n+1)} \tag{2}$$

where $B = 2K_{IC}^2/A\Omega^2(n-2)$ with Ω being a crack geometry factor in the expression of $K_I = \Omega\sigma\sqrt{a}$ with σ being a remote applied stress, and σ_m is the inert strength. By taking the logarithm both sides of Equation 2 yields

$$\log\sigma_f = \frac{1}{n+1}\log\dot{\sigma} + \log D \tag{3}$$

where $\log D = [1/(n+1)]\log[B(n+1)\sigma_m^{n-2}]$. The SCG parameter n can be obtained from the slope of Equation 3 by using a linear regression analysis of $\log\sigma_f$ versus $\log\dot{\sigma}$. The parameter A is determined from the intercept (D) together with appropriate constants. Equation 2 is the commonly utilized, one-dimensional SCG ("dynamic fatigue") solution for the "infinite" body where stress intensity factor along the crack front is uniform at a given time during crack growth.

The stress-intensity factor solution for a surface crack in a plate with finite thickness (see Fig. 1) has been developed by Newman and Raju [13], and has been widely used to determine fracture toughness of materials and fatigue crack growth for metallic materials. The resulting stress intensity factor for flexure load is

$$K_I = H\sigma\sqrt{\frac{\pi a}{Q}}F\left(\frac{a}{w}, \frac{a}{c}, \frac{c}{b}, \phi\right) \tag{4}$$

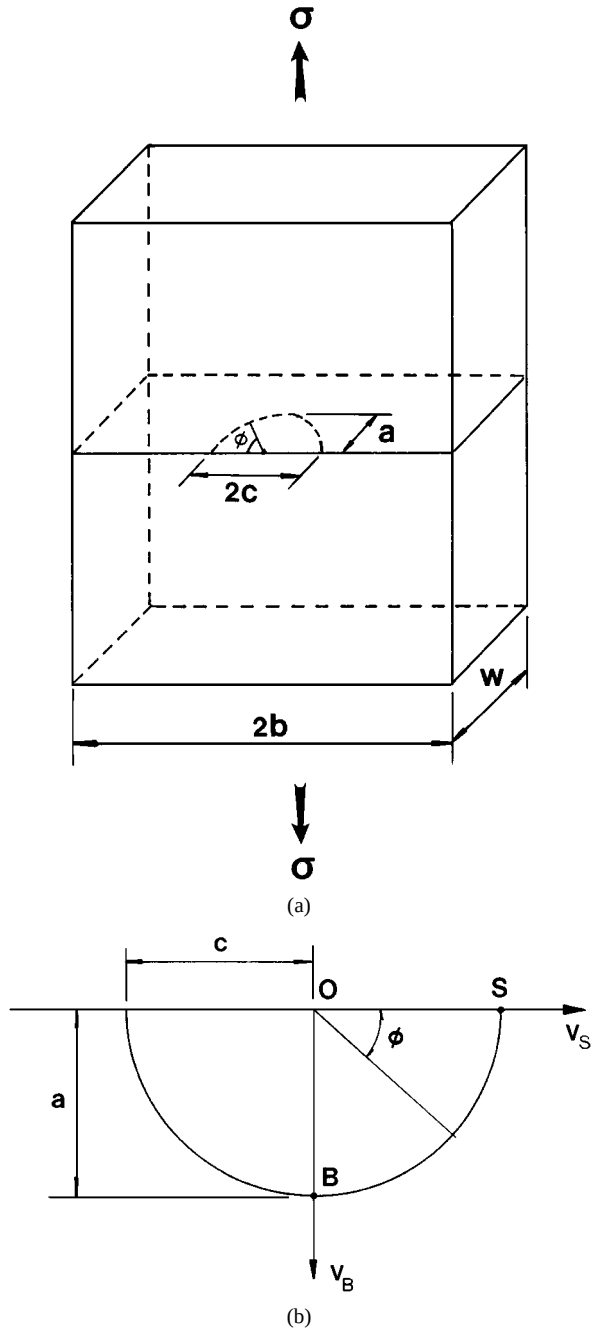

Figure 1 Crack geometry: (a) surface crack configuration in a finite specimen; (b) a surface crack during slow crack growth representing crack velocities at the surface (at 'S') and at the depth (at 'B').

for $0 \le a/w < 1.0$, $0 \le a/c \le 1.0$, $c/b < 0.5$ and $0 \le \phi \le \pi$. σ is the remote outer-fiber flexural stress. The functions H, Q and F are complex in expression, and are dependent on crack geometry and specimen dimensions (see Appendix). A new crack geometry factor, Y, was used for simplicity as follows:

$$Y \equiv \frac{HF}{\sqrt{Q}} \tag{5}$$

The slow crack velocity for a given material/ environment condition depends on stress intensity factor as shown in Equation 1. For an infinite body the crack velocity of a semicircular surface crack is all the same along the crack front. However, as the crack length becomes comparable to the specimen thickness, the stress

intensity factor is no longer identical along the crack front: The maximum and minimum stress intensity factors occur, respectively, at the surface and at the depth, due to the stress gradient through the specimen thickness [13]. This gives rise to a change in crack velocity at the crack front, resulting in crack-shape change (into an ellipse) during slow crack growth. Based on Equation 1, the individual crack velocities both at the surface (at 'S') and the depth (at 'B') of a crack (see Fig. 1b) can be expressed

$$\begin{aligned} v_S &= \frac{dc}{dt} = A\left(\frac{K_{IS}}{K_{IC}}\right)^n \\ v_B &= \frac{da}{dt} = A\left(\frac{K_{IB}}{K_{IC}}\right)^n \end{aligned} \tag{6}$$

where v_S and v_B are the crack velocities at the surface and at the depth, respectively, and K_{IS} and K_{IB} are the SIF's at the surface and at the depth. The SCG parameters n and A can be assumed invariant since the parameters are the constants for a given material/environment system. From Equations 4 and 5, the corresponding stress intensity factors at the surface and the depth become

$$\begin{aligned} K_{IS} &= Y(\phi = 0)\,\sigma\sqrt{\pi a} \\ K_{IB} &= Y\left(\phi = \frac{\pi}{2}\right)\sigma\sqrt{\pi a} \end{aligned} \tag{7}$$

The critical stress intensity factor for a semicircular crack can be expressed using Equations 4 and 5 with $\phi = 0$ (where a maximum SIF occurs) as follows:

$$K_{IC} = Y_m(\phi = 0)\,\sigma_m\sqrt{\pi a_m} \tag{8}$$

where Y_m and a_m are, respectively, crack geometry factor and crack depth in the inert condition whereby no slow crack growth occurs. Hence, a_m corresponds to the initial crack size.

The analytical solution of Equations 6 and 7 in terms of failure strength as a function of stress rate is not feasible because of two-dimensional crack growth, coupled with a great complexity of the time-varying stress intensity factors associated with Y (see Appendix) as a crack grows. A two-dimensional solution has to be made via numerical methods. To minimize the number of parameters to be specified (such as A, a_m, a, c, σ_m, σ, K_{IC} and t, etc.), it is convenient to utilize a normalized scheme, as used previously in the one-dimensional, slow-crack growth analysis of indentation-induced flaws [9, 11]. The normalized variables for the two-dimensional analysis were used as follows:

$$\begin{gathered} K_S^* = \frac{K_{IS}}{K_{IC}};\quad K_B^* = \frac{K_{IB}}{K_{IC}};\quad J = \frac{A}{a_m}t;\quad \sigma = \frac{\sigma}{\sigma_m}; \\ C_S = \frac{c}{a_m};\quad C_B = \frac{a}{a_m};\quad \dot\sigma^* = \frac{\sigma^*}{J} \end{gathered} \tag{9}$$

where K_S^*, K_B^*, J, σ^*, C_S, C_B and $\dot\sigma^*$ are, respectively, normalized stress intensity factors (at points 'S' and 'B' in Fig. 1b), normalized time, normalized applied stress, normalized crack sizes (at points 'S' and 'B'), and normalized stress rate. Using these variables, the normalized stress intensity factors and the normalized crack velocities at both points yield

$$\begin{aligned} \frac{dC_B}{dJ} &= \left[K_B^*\right]^n \\ \frac{dC_S}{dJ} &= \left[K_S^*\right]^n \\ K_B^* &= \frac{Y(\phi = \pi/2)}{Y_m}\dot\sigma^* J C_B^{1/2} \\ K_S^* &= \frac{Y(\phi = 0)}{Y_m}\dot\sigma^* J C_B^{1/2} \end{aligned} \tag{10}$$

The solutions of these equations including two simultaneous differential equations, in terms of normalized variables such as strength, failure time and crack sizes, were obtained by using the fourth-order Runge-Kutta method for a given n and stress rate ($\dot\sigma^*$). The two-dimensional analysis was performed for the crack to simultaneously grow both in the surface and in the depth directions, coupled at any instant of time with the geometry factor Y. The solution procedure was initiated to determine the normalized strength as a function of normalized stress rate for the selected values of $n = 5$–160. A range of normalized stress rates from $\dot\sigma^* = 1.0 \times 10^2$ to 1.0×10^{-7} was used. The initial condition was $C_S = C_B = 1$, that is, the crack starts growing from a semicircular crack configuration ($c/a = 1$). The instability conditions were $K_S^* = 1$ or $K_B^* = 1$, whichever occurs first, and $dK_S^*/dC_S > 0$ or $dK_B^*/dC_B > 0$. A set of four-different, normalized specimen thicknesses was used in the analysis: $T = 2$, 3.3, 10 and ∞, where T is the normalized thickness in which the specimen thickness (w) was normalized with respect to the initial crack size (a_i) as follows:

$$T = \frac{w}{a_i} \tag{11}$$

The program can be readily incorporated into the one-dimensional analysis once it is set to $v_S = v_B$. The following are the numerical results regarding strength vs. stress rate, SCG parameters, and crack shape.

2.1. Strength versus stress rate

A summary of the numerical solution of normalized strength ($\log \sigma_f^*$) as a function of normalized stress rate ($\log \dot\sigma^*$) in flexure is shown in Fig. 2. The figure is for a set of four different, normalized specimen thicknesses of $T = 2$, 3.3, 10 and ∞. Below $\dot\sigma^* = 10^{-1}$, there exists a linear relationship between $\log \sigma_f^*$ and $\log \dot\sigma^*$ for each n. Above $\dot\sigma^* = 10^1$, the strength converges to $\sigma_f^* = 1$ in which the inert strength is defined. It was found that for the infinite body ($T = \infty$) the solution exhibited no difference between the conventional, 1-D analysis (Equation 3) and the numerical two-dimensional analysis, since $K_{IS} = K_{IB}$ with $a/c = 1$ during the whole period of slow crack growth.

For $n \geq 20$, the curves among the four T's have no significant difference in slope and intercept. However,

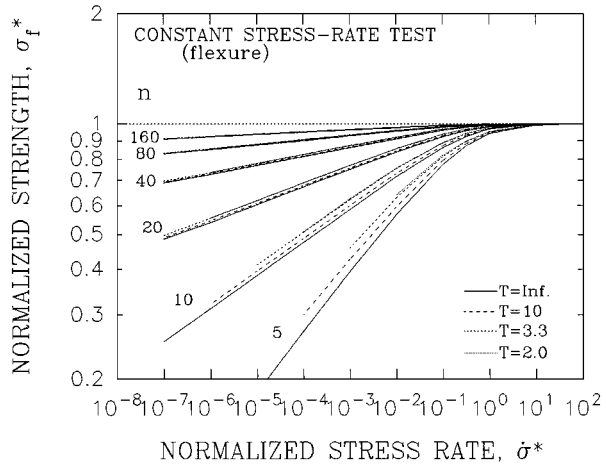

Figure 2 Results of the numerical solutions of normalized strength (σ_f^*) as a function of normalized stress rate ($\dot{\sigma}^*$) in flexure for different levels of normalized specimen thickness (T).

for $n \leq 10$, representing a condition of high SCG susceptibility, the deviation from the curve for $T = \infty$ is amplified with both decreasing specimen thickness T and decreasing n. This is ascribed to the accelerated crack growth in which the crack depth a becomes quickly comparable to the specimen thickness. The lower limit of $\dot{\sigma}^*$, $\dot{\sigma}_L^*$, below which no solution exists, corresponds to the condition of $C_B \approx T$ (or $a \approx w$) where a part-through crack configuration forms. The values of $\dot{\sigma}_L^*$, critical for $n \leq 10$, can be found from Fig. 1. For $n = 10$, $\dot{\sigma}_L^* \approx 10^{-4}$, 10^{-5}, and 10^{-7}, respectively, for $T = 2$, 3.3 and 10; whereas, for $n = 5$, $\dot{\sigma}_L^* \approx 10^{-2}$, 10^{-3}, and 10^{-4}. Therefore, the common use of at least four stress-rates, usually one decade apart, with a condition of $\dot{\sigma}^* \leq 10^{-1}$ is limited for the cases of $n \leq 5$ and $T \leq 3.3$.

2.2. Slow crack growth parameters

As seen in Fig. 2, below $\dot{\sigma}^* = 10^{-1}$, there exists a linear relationship between log σ_f^* and log $\dot{\sigma}^*$. Hence, analogous to the conventional infinite-body relation, Equation 3, a relationship can be expressed as follows [9, 11]:

$$\log \sigma_f^* = \frac{1}{n'+1} \log \dot{\sigma}^* + \log I \qquad (12)$$

where n' is the 'apparent' SCG parameter and I is the intercept. The 'apparent' SCG parameter n' was determined from the slope of the data in Fig. 2 by a linear regression analysis of log σ_f^* versus log $\dot{\sigma}^*$, based on Equation 12. The resulting plot of the 'apparent' SCG parameter n' as a function of n is shown in Fig. 3a. The variation in n' from n was greater for $n \leq 10$ and is increased with both decreasing T and decreasing n. The variation in n' was defined as $\Delta_n = (n' - n)/n$. A summary of Δ_n as a function of n for different T's is shown in Table I. For $n = 5$, $\Delta_n = 54$, 41 and 22%, respectively, for $T = 2$, 3.3 and 10. For $n = 10$, $\Delta_n = 14$, 9 and 5%, respectively, for $T = 2$, 3.3 and 10. For $n \geq 20$, the variation in n' was negligibly small with a maximum value of 4%, occurring for $T = 2$.

TABLE I The deviations (Δ_n and Δ_I) in slow crack growth parameters n' and I

Normalized specimen thickness, T	True slow crack growth parameter n					
	5	10	20	40	80	160
	(a) Δ_n					
2	0.54	0.14	0.04	0.02	0.01	0.01
3.3	0.41	0.09	0.03	0.02	0.01	—
10	0.22	0.05	0.02	0.01	—	—
∞	—	—	—	—	—	—
	(b) Δ_I					
2	−0.12	−0.02	−0.02	−0.01	—	—
3.3	−0.10	−0.01	−0.01	—	—	—
10	−0.09	−0.01	—	—	—	—
∞	—	—	—	—	—	—

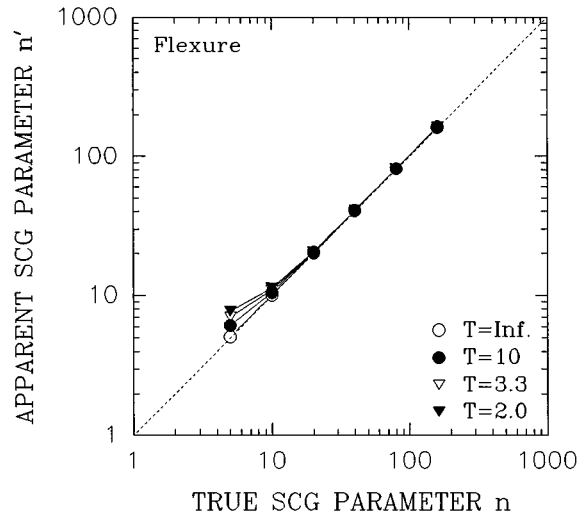

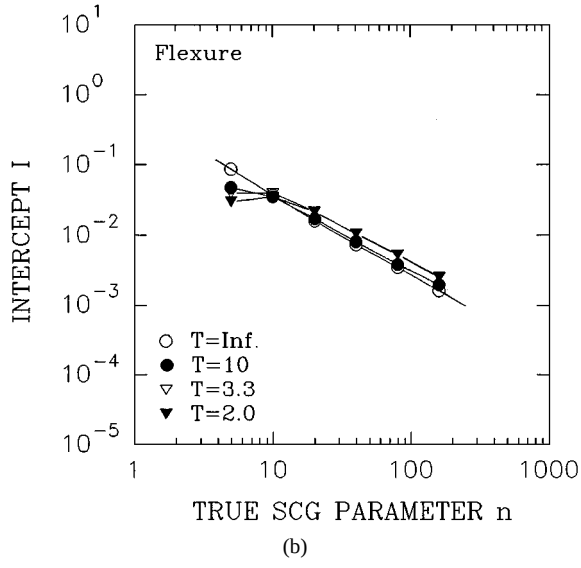

Figure 3 Results of the numerical solutions of slow crack growth parameters as a function of n in flexure for different levels of normalized specimen thickness (T): (a) for n' and (b) for log I.

A summary of the intercept based on the data in Fig. 2 and Equation 12 is shown in Fig. 3b and Table I. The overall variation in I from the solution for $T = \infty$, $\Delta_I = (I_{T=\infty} - I)/I$, was less insignificant, compared to Δ_n. For $n = 5$, the variation is $\Delta_I = 12$, 10 and 9% (all negative), respectively, for $T = 2$, 3.3 and 10. For

$n \geq 10$, the variation was negligible for all T's with a maximum value of -2%.

From the results shown in Fig. 3 and Table I, it is evident that in order to maintain a maximum variation of less than 10% in both n and I with at least four stress rates one must use the conditions of $n \geq 10$ and $T \geq 3.3$. For a maximum variation of 5%, the conditions of $n \geq 10$ and $T \geq 10$ must be fulfilled. In case of $n \geq 20$, one can use thin specimens with $T = 2.0$ (the initial crack size is 50% of the specimen thickness) with an error of about 4%. Since most glasses at ambient temperature and many advanced ceramics at elevated temperatures exhibit $n \geq 20$, the specimens fabricated from those materials containing initial crack sizes of 50% of the specimen thickness can be used to determine the SCG parameters with an error of 4% using the conventional, simple (1-D infinite-body) analytical solution (Equation 2 or 3).

2.3. Crack shapes

Typical examples of the numerical solution of critical crack size and its shape at failure are depicted in Fig. 4. The figure is for the cases of $n = 10$ and 20 with $T = 10$. Both the aspect ratio a/c and the crack-depth to specimen-thickness ratio a/w were plotted as a function of stress rate. The change in crack shape from the initial semicircle ($a/c = 1.0$) to ellipse is insignificant at higher stress rates. However, the change is significant at lower stress rates with decreasing n, attributed to enhanced slow crack growth. The corresponding a/w ratio increases with both decreasing stress rate and decreasing n. The crack depth at failure, for example, reaches about 80% of the specimen thickness for the case of extended slow crack growth, which is for $n = 10$ at $\dot{\sigma}^* = 1 \times 10^{-6}$.

A more detailed description of the accompanying crack-shape change *during slow crack growth* is shown in Fig. 5, where the aspect ratio (a/c) was plotted as a function of normalized time (J) for the cases of $n = 10$ and 20 with $T = 10$. Two stress rates, $\dot{\sigma}^* = 1 \times 10^{-3}$ and 1×10^{-6}, were considered in the analysis. At 1×10^{-3}, the initial semicircular crack grows to a slightly elliptical configuration with $a/c =$ 0.85 for

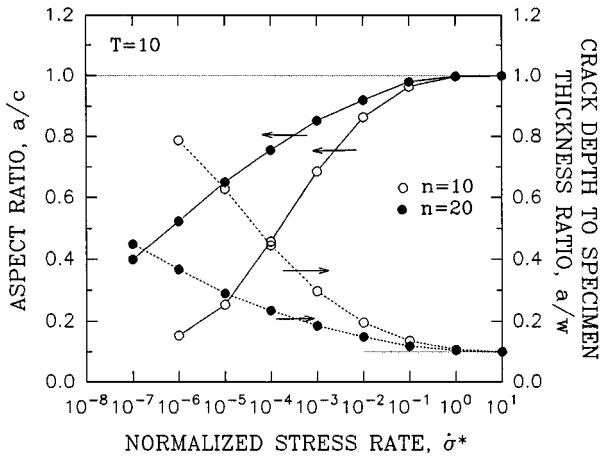

Figure 4 Results of the numerical solutions of crack configurations (a/c and a/w) at failure as a function of stress rate in flexure for $n = 10$ and 20 with a normalized specimen thickness of $T = 10$.

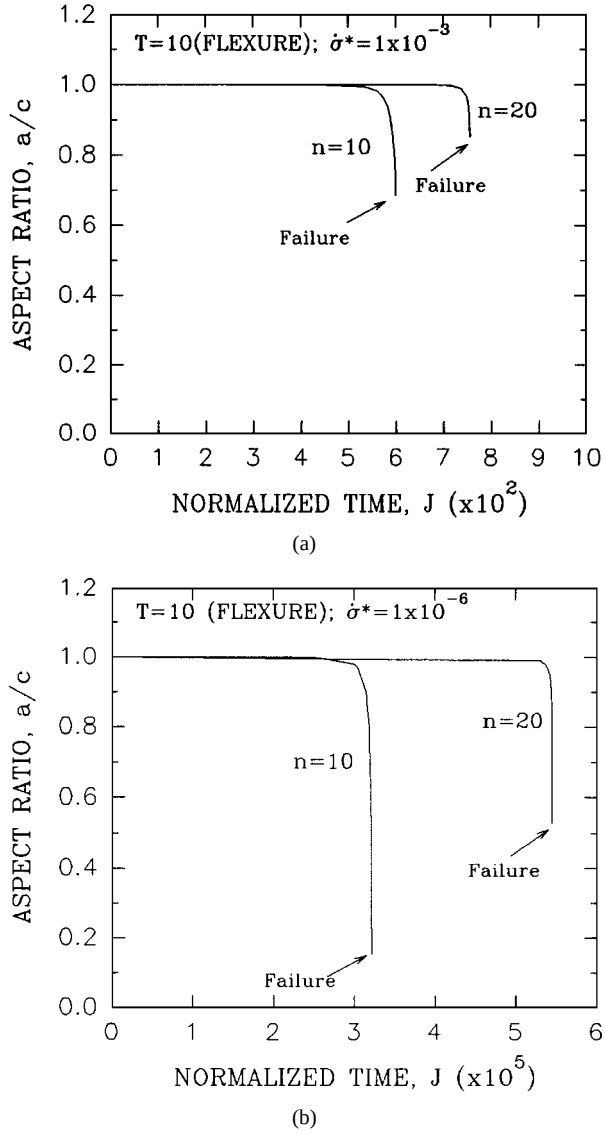

Figure 5 Results of the numerical solutions of crack growth (aspect ratio $= a/c$) as a function of normalized test time (J) in flexure with a normalized specimen thickness of $T = 10$ for $n = 10$ and 20: (a) For $\dot{\sigma}^* = 1 \times 10^{-3}$; (b) For $\dot{\sigma}^* = 1 \times 10^{-6}$.

$n = 20$; whereas, the crack grows considerably elliptical to a value of $a/c = 0.67$ for $n = 10$. The trend for 1×10^{-6} is similar; however, the ellipticity is much more magnified, compared to that for 1×10^{-3} because of extended slow crack growth. The resulting ellipticity at failure for 1×10^{-6} amounts to $a/c = 0.53$ and 0.15, respectively, for $n = 20$ and 10. It is noted from Fig. 5 that the initial crack grows very little during most of testing time, but grows instantaneously close to the failure time at which failure strength is defined. A long *incubation* time of an initial crack is a unique aspect for slow crack growth behavior of most brittle materials subjected to constant stress-rate testing [7].

For a given material/environment condition, the change in shape of an initial semicircular crack during slow crack growth is dependent on stress intensity factor at its crack front. In flexure, the stress gradient through specimen thickness is significant so that the stress intensity factor is smaller at the depth than at the surface when the crack length due to SCG increases toward the specimen thickness. This results in a faster crack

growth in the surface than in the depth direction, giving rise to the crack with an elliptical crack configuration. The ellipticity is more enhanced as the crack grows close to the bottom of the specimen (see Figs 4 and 5), with both decreasing stress rate and decreasing n. It is important to note that despite a significant change in crack shape during slow crack growth, the SCG parameters determined by the 2-D, finite-body numerical solution do not noticeably differ from those by the simple, 1-D, infinite-body analytical solution (Equation 3) for most glass and advanced ceramics ($n \geq 20$) provided that $T \geq 2$, as aforementioned in Section 2.2.

3. Experimental

In order to compare the numerical solutions with experimental data, constant stress-rate flexural ("dynamic fatigue") testing was conducted with soda-lime glass microslides in distilled water at room temperature. The glass microslides were used since this material exhibits a somewhat high SCG susceptibility ($n \approx 20$) in a moist environment and since the microslides provide an ideal thin plate configuration with low cost. The nominal dimensions of the glass microslides (No. 2954-F, Erie Scientific Co., Portsmouth, NH) were 1.2 mm by 25 mm by 75 mm, respectively, in thickness, width and length. Controlled-surface cracks were produced at the center of each specimen using a Vickers microhardness indenter (Model 3212, Zwick, Germany) with one of the indentation diagonals oriented along the direction of the prospective tensile stress of the specimen. Four different indentation loads ranging from $P = 2$ to 98 N were used. In order to avoid any complexity associated with the residual contact stresses produced by elastic/plastic indentation deformation, all the as-indented specimens were annealed at 520 °C in air for 20 h to remove the residual stresses.

Constant stress-rate testing for the indented-and-annealed specimens was carried out in an electromechanical testing machine (Model 8562, Instron, Canton, MA) using a stainless-steel, four-point flexure fixture with 20 mm-inner and 40 mm outer spans. Three to five stroke rates in displacement control, ranging typically from 0.0005 to 50 mm/min, corresponding to stress rates from 2.2×10^{-3} to 220 MPa/s, were employed at each indentation load. A total of four specimens were used at each test rate. This number of test specimens, four at each test rate, was considered statistically sufficient since the strength scatter (=coefficient of variation) exhibited less than 5%. The inert strength for each indentation load was also determined using silicon oil at a fast stress rate of 220 MPa/s.

From the indentation-fracture analysis [9] using $K_{IC} = 0.76$ MPa$\sqrt{\text{m}}$ and other known parameters [14], the normalized specimen thickness (Equation 11) was determined to be $T \approx$ 70, 40, 10, and 5, respectively, for the indentation loads of $P = 2$, 5, 39 and 98 N. It was observed that above $P = 98$ N the indent cracks tended to form more palmqvist or elliptical crack configurations (frequently with spalling) than semicircular, so that the indent load of $P = 98$ N was considered as a maximum load to produce semicircular surface radial/median crack configurations. Therefore, it was not possible in this experiment to achieve a normalized specimen thickness of less than 5 (e.g., $T < 5$), although the numerical analysis was covered up to $T = 2$.

4. Results and discusssion

A summary of the constant stress-rate flexural testing results for the soda-lime glass microslides with four different T's is shown in Fig. 6. The decrease in failure strength with decreasing stress rate, which represents the susceptibility to slow crack growth, was evident for all the normalized specimen thicknesses. The values of the SCG parameter n, determined by a linear regression analysis of log σ_f versus log $\dot{\sigma}$ based on Equation 3, were $n = 19.0 \pm 2.2$, 19.9 ± 2.4, 20.0 ± 0.5 and 17.0 ± 1.4, respectively, for $T = 70$, 40, 10 and 5 (or for $P = 2$, 5, 39 and 98 N).

An additional numerical analysis using $n = 19.0$ showed that there was no difference in SCG parameters (n and I) between the infinite-body ($T = \infty$) and the finite-body ($T = 70$) solutions. Therefore, the experimental data obtained from $T = 70$ can be regarded as those for the infinite-body condition, free from any effects on specimen thickness. Using Equations 2, 9 and 12 together with n (=19), I and appropriate parameters for $T = 70$, the SCG parameter A was determined to be $A = 1.6 \times 10^{-3}$ m/s. Now using the determined A and the value of I obtained numerically for each T with $n = 19.0$, one can predict from Equations 2, 9 and 12 failure strength as a function of stress rate for $T = 40$, 10 and 5.

The resulting prediction is shown in Fig. 6 with the dotted lines. The difference in n between the experimental data and the prediction ($n = 19.0$) was 5, 5, and −11%, respectively, for $T = 40$, 10 and 5; whereas, the respective difference in intercept was 2, 3, and 2%. Although the experimental value of $n = 17.0$ for $T = 5$ is a little lower than the values of $n = 19$–20 for $T \geq 10$ resulting in a difference of about 10%, the

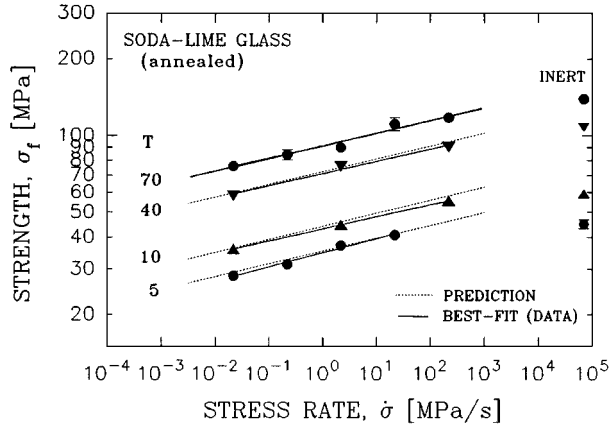

Figure 6 Results of constant stress-rate flexural testing for indented-and-annealed soda-lime glass microslides with four different normalized specimen thicknesses from $T = 5$ to 70 (corresponding indentation loads from $P = 2$ to 98 N) in room-temperature distilled water. The solid lines indicate the best-fit lines based on Equation 3; whereas, the dotted lines represent the predicted lines based on the data for $T = 70$. Error bar represents ± one standard deviation (the error bars smaller than symbols were omitted for clarity). The inert strengths were also plotted for comparison.

overall agreement between the experimental data and the prediction is reasonable within the range of experimental scatters. Note that even the average coefficient of variation in n for each T was about 9%. In fact, the obtained values of $n = 17$ to 20 from this study with a *wide* range of indentation loads from $P = 2$ to 98 N, agree well with those ($n = 18$–20) independently determined for soda-lime glass using primarily lower indentation loads ($P \leq 10$ N) by other investigators [10, 15, 16]. Thus, the result shown in Fig. 6 indicates that no appreciable difference in SCG parameters is evident between the 2-D, finite-body numerical solution and the conventional, simple 1-D, infinite-body analytical solution (Equation 2).

Alternatively but approximately, the effect of specimen thickness (T) on SCG parameters can be examined by constructing the universal failure strength-versus-stress rate relation based on the indentation-fracture analysis [15]. Multiplying both sides of Equation 2 by $P^{1/3}$ and arranging the terms yield the following relationship

$$\sigma_f P^{1/3} = \alpha[\dot{\sigma} P]^{1/(n+1)} \tag{13}$$

where $\alpha = [B(n+1)(\sigma_m P^{1/3})^{n-2}]^{1/(n+1)}$, which is constant for a given material/environment system regardless of indentation load since $\sigma_m P^{1/3}$ is constant according to the indentation analysis [10, 15]. An equation similar to Equation 13 has been used for the as-indented crack system in which a residual stress field is present about the indent [15]. The resulting plots of log $\sigma_f P^{1/3}$ as a function of log $\dot{\sigma} P$ using the data in Fig. 6 are depicted in Fig. 7. Each symbol represents a mean value for a total of four specimens. The solid line represents a best-fit line with $n = 19.0$. As can be seen in the figure, no appreciable trend for data at different indentation loads to deviate from universal behavior is evident. This indicates that the wide range of indentation loads from $P = 2$ to 98 N which were used in this study to produce the range of corresponding normalized specimen thicknesses from $T = 70$ to 5 resulted in no substantial effect of the specimen thickness T on the estimation of SCG parameters. (Note that based on the indentation-fracture analysis [10, 15], the initial as-indent crack size depends on indentation load: $a_i = \delta P^{3/2}$ with δ being a constant. This gives a relation of $T = w/a_i = w/\delta P^{3/2}$. Therefore, Equation 13 can also be expressed in terms of T by replacing P with T. The result using either P or T remains the same.)

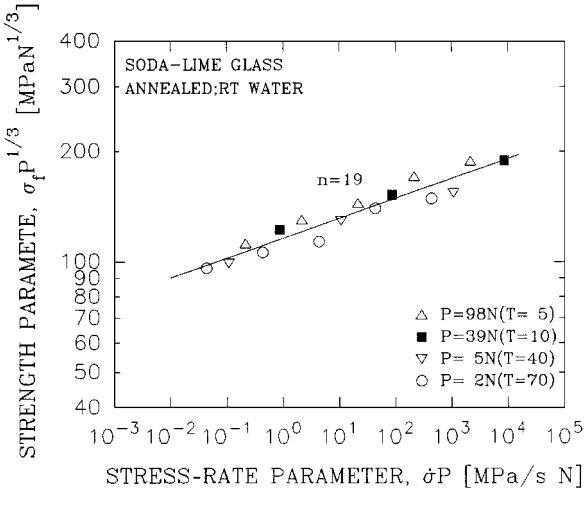

Figure 7 Strength parameter (log $\sigma_f P^{1/3}$) as a function of stress-rate parameter (log $\dot{\sigma} P$) for four T's obtained from the experimental data in Fig. 6. The solid line represents the best-fit line with $n = 19$.

From the fracture surface examinations of specimens tested at lower stress rates with low T's, it could be speculated that the cracks seemed to have grown to elliptical configurations, in view of the propagation mode of the Wallner lines. However, in most cases, it was difficult or impossible to identify the boundary of crack front at failure because of no clear demarcation between slow crack growth and dynamic crack propagation (mirror/mist/hackle regions), as is typical of most glasses. The numerical calculations of crack configurations at failure showed that particularly at the lowest stress rate ($=2.2 \times 10^{-2}$ MPa/s), the aspect ratio (a/c) was significant about 0.60 and 0.45, respectively, for $T = 10$ and 5, while the corresponding, respective crack depth reached about 30 and 50% of the specimen thickness. The elliptical crack formation in flexure has been observed more clearly for some ceramics subjected to elevated-temperature, constant stress-rate flexural testing, because of well-defined demarcation of SCG region [17, 18]. The formation of a crack into ellipticity in flexure also has been observed for metallic specimens under cyclic fatiguing [19–21].

Because of the limited experiments conducted in this study using soda-lime glass microslides exhibiting $n = 19$ with $T = 5$–70, the obtained numerical solutions for $T = 2$ and 3.3 with $n \leq 10$ could not be verified with experiment. In fact, it is rarely feasible to find a material with $n \leq 10$ at ambient temperature since glass, known most susceptible to slow crack growth, exhibits as much as $n \approx 20$. Although not certain, an alternative to approach such extreme conditions of $n \leq 10$ with $T < 5$ would be to utilize ceramics at *elevated temperatures* with an appropriate combination of material/thickness/test temperature under the condition that the material follows the power-law SCG, Equation 1. The most important conclusion drawn from this study is that in spite of the significant change in crack shape during slow crack growth in flexure, the conventional simple, one-dimensional infinite-body analytical solution (Equation 2 or 3) can be used with a reasonable accuracy to determine SCG parameters for finite thin specimens: Realistically (experimentally) for $n \geq 20$ and $T \geq 5$ and analytically for $n \geq 10$ and $T > 3.3$.

5. Conclusions

The effect of specimen thickness on the estimation of SCG parameters of brittle materials subjected to constant stress-rate flexural testing was determined by using a two-dimensional numerical solution. The numerical solution showed that the change in crack shape at failure was significant, forming considerable elliptical crack configurations particularly at both low stress rate and low T. Notwithstanding the significant change in crack shape together with appreciable crack

growth, the difference in SCG parameters between the two-dimensional numerical solution and the conventional, one-dimensional infinite-body analytical solution was negligible with a maximum error of about 5% for $T > 3.3$ (the initial crack size is less than 30% of the specimen thickness) with $n \geq 10$. The experimental data obtained from constant stress-rate flexural testing for soda-lime glass microslides with a limited range of $T = 5$–70 supported the numerical solutions within the experimental range employed.

Appendix: Expressions of *H*, *Q* and *F*

The functions H, Q and F are expressed as follows [13]:

For the function H:

$$H = H_1 + (H_2 - H_1)\sin^p\phi \tag{A1}$$

where

$$H_1 = 1 - 0.34\frac{a}{w} - 0.11\frac{a}{c}\left(\frac{a}{w}\right)$$

$$H_2 = 1 - \left(1.22 + 0.12\frac{a}{c}\right)\left(\frac{a}{w}\right) + \left[0.55 - 1.05\left(\frac{a}{c}\right)^{0.75} + 0.47\left(\frac{a}{c}\right)^{1.5}\right]\left(\frac{a}{w}\right)^2$$

$$p = 0.2 + \frac{a}{c} + 0.6\frac{a}{w}$$

For the function Q:

$$Q = 1 + 1.464\left(\frac{a}{c}\right)^{1.65} \tag{A2}$$

For the function F:

$$F = \left[M_1 + M_2\left(\frac{a}{w}\right)^2 + M_3\left(\frac{a}{w}\right)^4\right] f_\phi g f_b \tag{A3}$$

where

$$M_1 = 1.13 - 0.09\left(\frac{a}{c}\right)$$

$$M_2 = -0.54 + \frac{0.89}{0.2 + (a/c)}$$

$$M_3 = 0.5 - \frac{1.0}{0.65 + (a/c)} + 14\left(1.0 - \frac{a}{c}\right)^{24}$$

$$f_\phi = \left[\left(\frac{a}{c}\right)^2 \cos^2\phi + \sin^2\phi\right]^{1/4}$$

$$g = 1 + \left[0.1 + 0.35\left(\frac{a}{w}\right)^2\right](1 - \sin\phi)^2$$

$$f_b = \left[\sec\left(\frac{\pi c}{2b}\sqrt{\frac{a}{w}}\right)\right]^{1/2}$$

The crack geometry factor Y, Equation 5, is expressed

$$Y = \frac{HF}{\sqrt{Q}} \tag{A4}$$

During slow crack growth both a and c are changing with time, hence, Y is a very complex function of time so that the only solution of slow crack growth is to use a numerical analysis on the basis of the governing differential equations.

Acknowledgements

The authors are thankful to Mr. R. Pawlik for the experimental work during the course of this study. This work was sponsored in part by the Ceramic Technology Project, DOE Office of Transportation Technologies, under contract DE-AC05-84OR21400 with Martin Marietta Energy System, Inc.

References

1. A. G. EVANS, *Int. J. Fract.* **10** (1974) 252.
2. G. G. TRANTINA, *J. Amer. Ceram. Soc.* **62** (1979) 377.
3. D. KALISH and B. K. TARIYAL, *ibid.* **61** (1978) 518.
4. R. K. GOVILA, "Ceramic Life Prediction Parameters," AMMRC TR 80-18, Army Material and Mechanics Research Center, Watertown, MA, 1980 (U.S. Department of Energy).
5. P. K. KHANDELWAL, J. CHANG and P. W. HEITMAN, in "Fracture Mechanics of Ceramics," Vol. 8, edited by R. C. Bradt, A. G. Evans, D. P. H. Hasselman, and F. F. Lange (Plenum Press, NY, 1986) p. 351.
6. J. P. SINGH, A. V. VIRKAR, D. K. SHETTY and R. S. GORDON, in "Fracture Mechanics of Ceramics," Vol. 8, edited by R. C. Bradt, A. G. Evans, D. P. H. Hasselman, and F. F. Lange (Plenum Press, NY, 1986) p. 273.
7. S. R. CHOI and J. A. SALEM, *J. Amer. Ceram, Soc.* **79** (1996) 1228.
8. "Standard Test Method for Determination of Slow Crack Growth Parameters of Advanced Ceramics Using Constant Stress-Rate Flexural Testing," ASTM C 1368, Annual Book of ASTM Standards, Vol. 15.01 (American Society for Testing and Materials, Philadelphia, PA, 1998).
9. B. R. LAWN, D. B. MARSHALL, G. R. ANSTIS and T. P. DABBS, *J. Mater. Sci.* **16** (1981) 2846.
10. E. R. FULLER, B. R. LAWN and R. F. COOK, *J. Amer. Ceram. Soc.* **66** (1983) 314.
11. S. R. CHOI, J. E. RITTER and K. JAKUS, *ibid.* **73** (1990) 268.
12. S. M. WIEDERHORN, in "Fracture Mechanics of Ceramics," Vol. 2, edited by R. C. Bradt, D. P. H. Hasselman, and F. F. Lange (Plenum, NY, 1978) p. 613.
13. J. C. NEWMAN and I. S. RAJU, *Eng. Fract. Mech.* **15** (1981) 185.
14. S. R. CHOI and J. A. SALEM, *Mater. Sci. Eng.* **A149** (1992) 259.
15. T. P. DABBS, B. R. LAWN and P. L. KELLY, *Phys. Chem. Glasses* **23** (1982) 58.
16. J. E. RITTER, M. VICEDOMINE, K. BREDER and K. JAKUS, *J. Mater. Sci.* **20** (1985) 2868.
17. S. R. CHOI, N. N. NEMETH, J. A. SALEM, L. M. POWERS and J. P. GYEKENYESI, *Ceram. Eng. Sci. Proc.* **16** (1995) 509.
18. S. R. CHOI, *J. Mater. Sci. Lett.* (1999), in press.
19. D. L. CORN, *Eng. Fract. Mech.* **3** (1971) 45.
20. W. S. PIERCE and J. L. SHANNON, *J. Test. & Eva.* **6** (1978) 183.
21. R. M. ENGLE, in "ASTM STP 687," edited by J. B. Chang (American Society for Testing and Materials, Philadelphia, 1979) p. 74.

Received 30 September 1998
and accepted 11 February 1999